Reactivity of nitrogen atoms from Zif-8 structure deposited over Ti 3 C 2 MXene in the electrochemical nitrogen reduction reaction

André Marinho, Clément Comminges, Aurélien Habrioux, Stéphane Célérier, Nicolas Bion, Cláudia Morais

Reactivity of Nitrogen Atoms from Zif-8 Structure Deposited over Ti_3C_2 MXene in the Electrochemical Nitrogen Reduction Reaction

André L. A. Marinho*[a], Clément Comminges[a], Aurélien Habrioux[a], Stéphane Célérier[a], Nicolas Bion[a], Cláudia Morais[a]

[a]*Institut de Chimie des Milieux et Matériaux de Poitiers (IC2MP), University of Poitiers, CNRS UMR 7285, TSA51106 – F86073, Poitiers Cedex 9, France.*

The electrochemical nitrogen reduction (NRR) to produce NH_3 is the most efficient, eco-friendly and cost-effective alternative to the Haber-Bosch process. It is crucial to investigate and develop electrocatalysts selective for NH_3 synthesis. In recent studies, the Ti_3C_2 MXene has emerged as a highly promising electrocatalyst for the NRR process. In this work, we explore the effect of Zif-8 addition over Mxene sheets in order to control the rate of hydrogen evolution reaction (HER). Despite the better result obtained for Zif-8@Ti_3C_2 (3.0 µg $NH_3.g_{cat}^{-1}.h^{-1}$ at -0.55 V/RHE), the ammonia produced when using Zif-8@Ti_3C_2 as cathode material is shown to be originated from nitrogen atoms contained in the Zif-8 structure instead of those of N_2. The results shed light to the need to fully understand the N_2 electroreduction process over N-containing electrocatalysts.

The development of low-carbon hydrogen production technologies requires a special attention toward the hydrogen storage, until now highly costed and dangerous due to the high pressure applied[1]. The use of ammonia (NH_3) as a liquid hydrogen carrier at ambient conditions appears as a promising alternative, however its production process (the Haber-Bosch process) demands a high energy consumption being one of the most CO_2 emitter process in the industry (4200 MT $year^{-1}$)[2]. Therefore, novel routes more sustainable must be developed and the N_2 electroreduction reaction (NRR) appears as a promising alternative. In the NRR process, ammonia is produced at ambient condition of temperature and pressure from N_2 and water in the presence of a catalyst through electricity, that can be supplied by renewable process generation (wind or solar) at decentralized points, avoiding large infrastructure investments[3]. This green ammonia process model has gained more attention in the past years, increasing from year to year the number of NRR-related publications.

The MXenes, a family of 2D compounds[4], appeared as a new type of material with outstanding characteristics for electrochemical applications and their performance

towards NRR has been evaluated in the last years[5,6]. Among the different MXenes studied in the literature, the Ti_3C_2 is the most evaluated in different electrochemical applications[7]. However, it is also active for H_2 evolution reaction (HER)[8], decreasing substantially the selectivity of the catalyst for NH_3 production. One strategy to inhibit HER and hence favor NRR is to increase the hydrophobicity of the MXene by the insertion of hydrophobic structures over its surface, such as the Zeolitic Imidazolate Framework (Zif), a sub-class of porous Metal-Organic-Frameworks (MOF)[9].

The appropriate interface MOF-MXene takes the advantages of MOF's structure, such as high porosity[10,11]. Moreover, the synergy between the different active sites improves the charge transfer in the material to be applied as electrocatalyst[12–14]. Recently, Liang et al.[5] demonstrated the better performance of Zif-67@Ti_3C_2 in comparison to Ti_3C_2 due to the higher hydrophobicity of Zif-67 structure, composed of Co, C, H and N.

In the last years, many works were published with N-containing catalysts presenting outstanding performances in the NRR. However, the presence of nitrogen atoms in the catalyst could be an additional source of N atoms for NH_3 production, instead of N_2 reduction[15], questioning the real performance of the catalyst. The infancy stage of the process and the absence of benchmarking protocol is still a challenge, resulting in contradictory results found in literature[3,16–18]. Many of them are caused by errors in the NH_3 quantification at sub-ppm scale due to the high sensibility of interfering species[3,19]. Herein, we examined the catalytic activity of Zif-8@Ti_3C_2 material for the NRR and we quantified the NH_3 production by UV-VIS technique, the most used technique nowadays. It is herein revealed that the NH_3 produced during the electrolysis emanates in fact from N atoms of the Zif-8 structure instead of those of N_2.

The Ti_3C_2 MXene was synthesized by etching of Al of parent Ti_3AlC_2 MAX phase using a LiF-HCl route as described in literature[8]. The XRD data (Figure S1) shows the shift of the peak at 2θ of the initial MAX phase from 9.6 to 7.0° due to both the removal of Al atoms in the MAX phase and the insertion of terminal groups (mixture of –OH, -O and –F), Li cations and water molecules[8]. The complete disappearance of the 002 peak of the initial MAX phase attests the formation of Ti_3C_2 MXene free of the precursors. The addition of Zif-8 results in an increase of the interlayer distance (increase of d_{002}) followed by the appearance of low intensities peaks ascribed to Zif-8 phase. The Raman spectrum of Ti_3C_2 shows the typical bands of MXene structure with –OH terminal groups[8]. The addition of Zif-8 does not change

the MXene structure and additional bands appeared at 168 cm^{-1}, 686 cm^{-1}, 1146 cm^{-1} and 1458 cm^{-1} corresponding to Zn−N stretching, imidazole ring puckering, C5−N stretching and methyl bending[20], respectively (Figure S2). Moreover, the SEM images with EDX mapping (Figure 1) shows the formation of Zif-8 over the MXene sheets, in accordance to the XRD and Raman results. Our previous work have demonstrated that the LiF-HCl route is responsible to produce MXenes with higher distance between sheets in comparison to the classical HF route[8]. Therefore, the Zif-8 insertion between the sheets is more likely. Then, we can conclude that the Zif-8 structure grew over the MXene sheets.

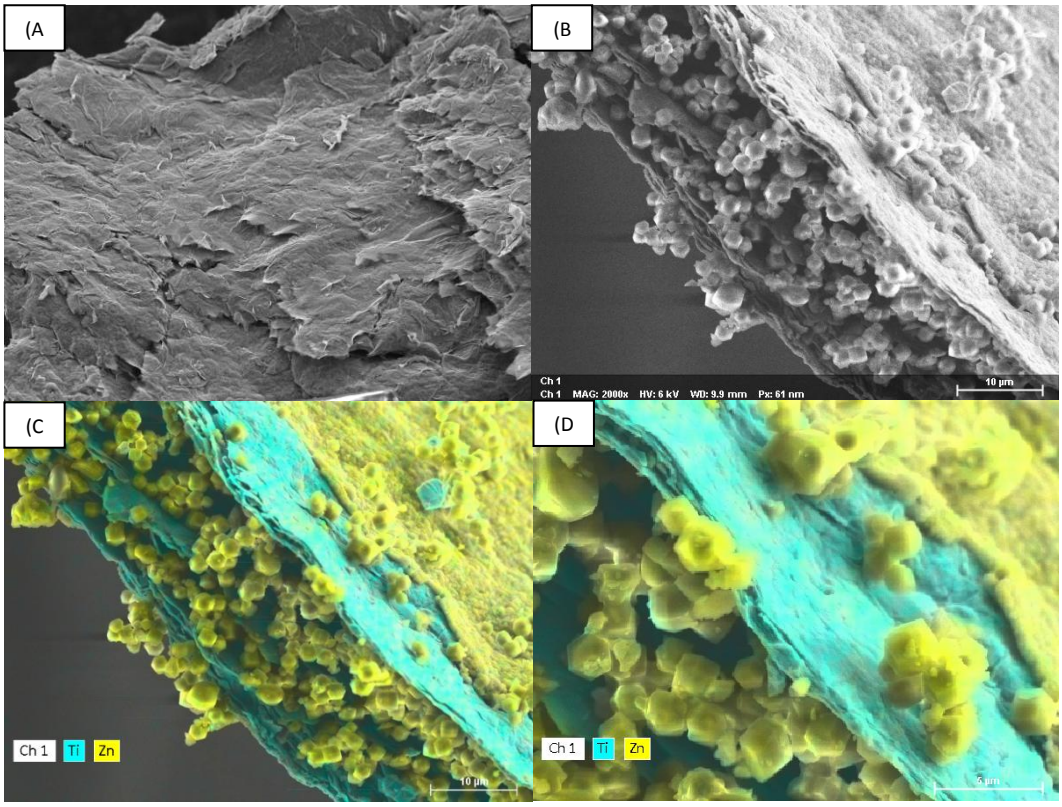

Figure 1. SEM images of (A) Ti_3C_2 MXene and (B) Zif-8@Ti_3C_2 composite. (C, D) EDX analysis of Zif-8@Ti_3C_2 mapping Zn and Ti as representative elements of Zif-8 and MXene, respectively.

The Zif-8@Ti_3C_2 was evaluated and compared with Ti_3C_2 for the NRR at ambient conditions. In order to decrease the H_2 evolution side reaction, the NRR was performed in a 0.1 M NaOH (pH = 14) electrolyte. The Fig. 2a shows the linear sweep voltammetry (LSV) curves recorded under Ar and N_2-saturated electrolyte for both materials. As shown, a slightly higher activity under N_2 atmosphere is observed, which can be attributed to the N_2 reduction. At 0.0 V/RHE the Ti_3C_2 catalyst presents already a low current density due to its higher double-layer capacitance of MXene materials

(Figure S3). Moreover, it is observed that the onset potential is shifted to lower potentials values for Zif-8@Ti_3C_2 as compared to Ti_3C_2. Indeed, the presence of Zif-8 over MXene surface modifies the accessibility of H_2O molecules to the electrocatalyst surface, reducing the rate of HER in comparison to Ti_3C_2 MXene for the same applied

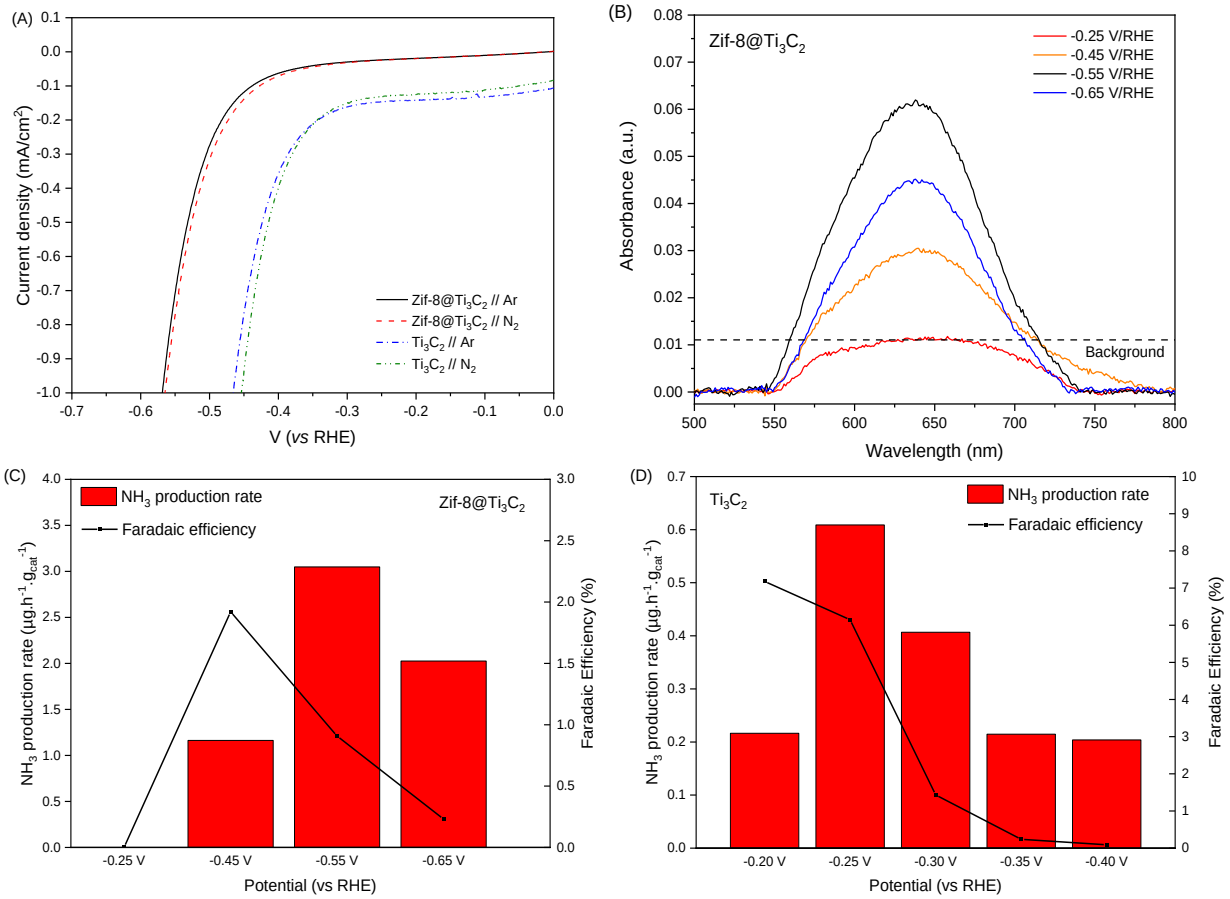

Figure 2. (A) LSV curves for Ti_3C_2 and Zif-8@Ti_3C_2 catalysts under Ar and N_2-saturated 0.1 M NaOH recorded at 10 mV/s; (B) UV-VIS spectra of electrolyte after 2 h of reaction at different potentials for Zif-8@Ti_3C_2 catalyst; (C); NH_3 production rate and faradaic efficiency of the Zif-8@Ti_3C_2 catalyst at different potentials; (D) NH_3 production rate and faradaic efficiency of the Ti_3C_2 catalyst at different potentials.

potential value.

In addition, the materials were submitted to cyclic voltammograms at high potential (0.4 to 2.0 V/RHE). At this condition, the Ti_3C_2 suffers irreversible oxidation to TiO_2 in alkaline medium and an oxidation peak is observed around 0.8 – 1.0 V vs RHE for both samples. The Ti_3C_2 MXene presents an oxidation peak much more intense than the Zif-8@Ti_3C_2 composite, evidencing the higher electrochemical surface area of the Ti_3C_2 MXene without Zif-8 addition, which constitutes another proof of the presence of Zif-8.

In order to proceed to NH_3 quantification, electrolysis were performed during 2 hours under N_2-saturated 0.1 M NaOH at different controlled potentials (Figure S5) for both

catalysts. For Zif-8@Ti_3C_2, it is possible to observe a dramatic change in the current density from -2.0 mA.cm^{-2} at -0.55 V/RHE to -4.5 mA.cm^{-2} at -0.65 V/RHE, thought a decrease in the NH_3 measured after reaction is observed (Figure 2b), which can be explained by the favoring of the HER at higher overpotential values.

The amount of produced NH_3 was determined by the UV-VIS analysis and, assuming that the NH_3 detected in the electrolyte originates from N_2 reduction, the highest NH_3 formation rate, up to 3.0 µg $NH_3.g_{cat}^{-1}.h^{-1}$, is obtained at -0.55 V/RHE with Zif-8@Ti_3C_2 catalyst (Figure 2c). Comparing the Ti_3C_2 and Zif-8@Ti_3C_2 catalysts, it is observed that the addition of Zif-8 increases the amount of NH_3 detected in the electrolyte after the reaction. The NH_3 formation rate increases from 0.6 µg $NH_3.g_{cat}^{-1}.h^{-1}$ for Ti_3C_2 at -0.25V/RHE, to 3.0 µg $NH_3.g_{cat}^{-1}.h^{-1}$ for Zif-8@Ti_3C_2 at -0.55 V/RHE (Figure 2d), as also demonstrated by other authors[5,21]. As demonstrated in the Fig. S6, no hydrazine is detected after NRR test at optimized potential and only NH_3 is produced from N_2 electrochemical reduction. Moreover, the Ti_3C_2 was shown to present a high chemical stability during 30 h of electrolysis, not showing any deactivation during this period (Figure S7).

The control tests are necessary to reveal the origins of N atoms from produced NH_3 during the electrochemical test under N_2-saturated electrolyte. In order to confirm the source of produced NH_3, electrolysis was also performed at the optimal potential value for each catalyst under Ar-saturated electrolyte and the obtained results are shown in the Figure 3. As expected, the Ti_3C_2 catalyst did not show any signal in the UV-VIS spectra above the background signal. However, the Zif-8@Ti_3C_2 presented a considerable increase of the UV-Vis absorbance, suggesting the presence of NH_3 in the electrolyte even without dissolved N_2. We also investigated the possibility of material decomposition on electrolyte by performing the NH_3 quantification after the electrodes were immersed 2 h into the electrolyte at open circuit potential (OCP) and in both cases, no ammonia was detected. These results suggest therefore that part of produced NH_3 during the electrolysis is being produced from the N atoms of the Zif-8 structure, which ones are inactive at OCP but are activated at reducing potentials, in the presence of H_2, since we observe different NH_3 production rates at different potential values. Therefore, it is not possible to correlate the Zif-8 hydrophobicity to its better performance towards NRR, since a considerable part of NH_3 originates from the catalyst itself.

The observed NH_3 production over Zif-8@Ti_3C_2 in Ar-saturated electrolyte lead us to conclude that the strategy proposed herein must be adopted for N-containing catalysts in

general, for which many recent works have demonstrated high performances towards the NRR. As long as the NH_3 production is still at sub-ppm levels, the possibilities of contamination must be carefully evaluated, especially when using N-containing materials as NRR catalysts, to avoid overestimated results. The utilization of ion chromatography and magnetic resonance techniques are still not applicable due to the very low amount of

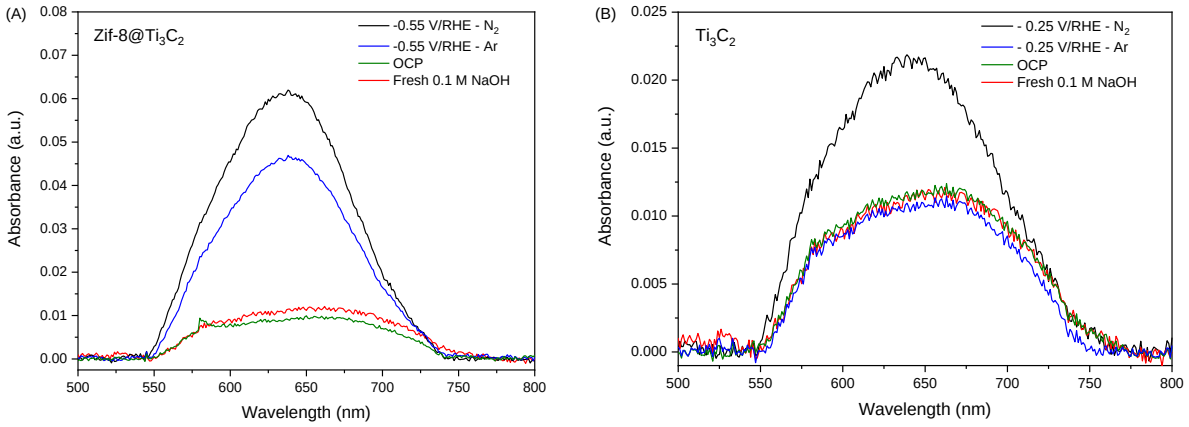

Figure 3. UV-VIS spectra of (A) Zif-8@Ti_3C_2 and (B) Ti_3C_2 catalysts after electrolysis under Ar and N_2-saturated 0.1 M NaOH and at open circuit potential (OCP).

produced NH_3. Moreover, it is mandatory to develop more sensitive techniques, preferentially *operando*, to quantify the amount of NH_3 and reveal the reaction mechanism, decreasing the influence of contaminants in the published results.

The authors gratefully acknowledge the Regional Council of Nouvelle Aquitaine (Neo Ammonia project, N°AAPR2020-2019-8018010), the CNRS (PEPS Energie BFC 220161), the French Ministry of Research and the European Regional Development Fund (ERDF) for financial supports.

Conflicts of interest

The authors declare no competing financial interest.

Notes and references

1 E. Rivard, M. Trudeau and K. Zaghib, *Materials*, 2019, **12**, 1973.

2 C. Tang and S.-Z. Qiao, *Chem. Soc. Rev.*, 2019, **48**, 3166–3180.

3 H. Liu, N. Guijarro and J. Luo, *J. Energy Chem.*, 2021, **61**, 149–154.

4 A. VahidMohammadi, J. Rosen and Y. Gogotsi, *Science*, 2021, **372**, eabf1581.

5 X. Liang, X. Ren, Q. Yang, L. Gao, M. Gao, Y. Yang, H. Zhu, G. Li, T. Ma and A. Liu, *Nanoscale*, 2021, **13**, 2843–2848.

6 J. Xia, H. Guo, G. Yu, Q. Chen, Y. Liu, Q. Liu, Y. Luo, T. Li and E. Traversa, *Catal. Lett.*, 2021, **151**, 3516–3522.

7 T.-Y. Shuai, Q.-N. Zhan, H.-M. Xu, C.-J. Huang, Z.-J. Zhang and G.-R. Li, *Chem. Commun.*, 2023, **59**, 3968–3999.

8 M. Benchakar, L. Loupias, C. Garnero, T. Bilyk, C. Morais, C. Canaff, N. Guignard, S. Morisset, H. Pazniak, S. Hurand, P. Chartier, J. Pacaud, V. Mauchamp, M. W. Barsoum, A. Habrioux and S. Célérier, *Appl. Surf. Sci.*, 2020, **530**, 147209.

9 T. Yu, S. Li, L. Zhang, F. Li, J. Wang, H. Pan and D. Zhang, *J. Colloid Interface Sci.*, 2023, **629**, 546–558.

10 H.-Y. Li, X. Hua, T. Fu, X.-F. Liu and S.-Q. Zang, *Chem. Commun.*, 2022, **58**, 7753–7756.

11 L. Zhang, C. Li, F. Li, S. Li, H. Ma and F. Gu, *Microchim. Acta*, 2022, **190**, 24.

12 T. Wang, P. Wang, W. Zang, X. Li, D. Chen, Z. Kou, S. Mu and J. Wang, *Adv. Funct. Mater.*, 2022, **32**, 2107382.

13 R. Paul, Q. Zhai, A. K. Roy and L. Dai, *Interdiscip. Mater.*, 2022, **1**, 28–50.

14 L. Zhang, J. Zhu, X. Li, S. Mu, F. Verpoort, J. Xue, Z. Kou and J. Wang, *Interdiscip. Mater.*, 2022, **1**, 51–87.

15 B. Hu, M. Hu, L. Seefeldt and T. L. Liu, *ACS Energy Lett.*, 2019, **4**, 1053–1054.

16 Z. Geng, Y. Liu, X. Kong, P. Li, K. Li, Z. Liu, J. Du, M. Shu, R. Si and J. Zeng, *Adv. Mater.*, 2018, **30**, 1803498.

17 S. Z. Andersen, V. Čolić, S. Yang, J. A. Schwalbe, A. C. Nielander, J. M. McEnaney, K. Enemark-Rasmussen, J. G. Baker, A. R. Singh, B. A. Rohr, M. J. Statt, S. J. Blair, S. Mezzavilla, J. Kibsgaard, P. C. K. Vesborg, M. Cargnello, S. F. Bent, T. F. Jaramillo, I. E. L. Stephens, J. K. Nørskov and I. Chorkendorff, *Nature*, 2019, **570**, 504–508.

18 J. Choi, H.-L. Du, C. K. Nguyen, B. H. R. Suryanto, A. N. Simonov and D. R. MacFarlane, *ACS Energy Lett.*, 2020, **5**, 2095–2097.

19 L. F. Greenlee, J. N. Renner and S. L. Foster, *ACS Catal.*, 2018, **8**, 7820–7827.

20 G. Kumari, K. Jayaramulu, T. K. Maji and C. Narayana, *J. Phys. Chem. A*, 2013, **117**, 11006–11012.

21 Y. Liu, X. Meng, Z. Zhao, K. Li and Y. Lin, *Nanomaterials*, 2022, **12**, 2964.